

# Smelting of different hydrogen-reduced bauxite residue-calcite pellets for iron and alumina recovery

*Manish Kumar Kar<sup>1</sup> and Jafar Safarian<sup>1</sup>*

1. Ph.D. Researcher, Department of Materials Science and Engineering, NTNU,7041 Trondheim, Norway: manish.k.kar@ntnu.no
2. Professor, Department of Materials Science and Engineering, NTNU,7041 Trondheim, Norway: jafar.safarian@ntnu.no

Keywords: bauxite residue, calcite, pelletizing, hydrogen reduction, smelting, iron, calcium-aluminate slag, alumina

## ABSTRACT

Bauxite residue is one of the most important byproducts from the alumina industry with no commercial use till now. The utilization of bauxite residue through pelletizing with different lime additions, hydrogen reduction, and smelting has been studied in this work. Three different types of green pellets were made with varying calcite-to-bauxite residue ratio and subsequently sintered at elevated temperatures. The sintered pellets were isothermally reduced at 1000 °C under hydrogen gas followed by smelting of the reduced pellets in argon at 1500 °C. Smelting of the reduced pellets leads to the recovery of metallic iron and the formation of a leachable calcium aluminate slag. XRD and SEM were used to characterize the phases and microstructural analysis. The iron produced in the smelting process has a high purity, above 99.5 wt.%. While the iron content of the slags is quite low, and the slags shows variations of krotite ( $\text{CaAl}_2\text{O}_4$ ), gehlenite ( $\text{Ca}_2\text{Al}_2\text{SiO}_7$ ), and perovskite ( $\text{CaTiO}_3$ ) phases based on the variation of calcite addition. It was found that the more calcite addition in pelletizing yields higher percentage of krotite phase as compared to lower calcite-containing pellets. Employing quantitative XRD analysis, the krotite phase fraction was found approximately 85 wt.% for higher calcite-added pellet, and around 74 wt.% for lower calcite-added pellet. Factsage thermodynamic software was used to evaluate the obtained experimental data, they both revealed that the components of the bauxite residue are mostly distributed into the calcium aluminate slag phase.

## 1. INTRODUCTION

As society undergoes continuous modernization, there is a concurrent rise in the demand for iron metal. However, the quality of traditional iron ore has seen a decline over time. Consequently, iron manufacturers are compelled to explore alternative secondary resources to meet the escalating demand. One such secondary source is bauxite residue, which boasts iron oxide content ranging from 40 to 60 wt.% [1][2]. Certainly, during the Bayer process, which is employed in the production of alumina from bauxite ore, red mud byproduct is generated. This red mud consists of undigested oxides and other impurities that remain after the extraction of alumina from the bauxite ore. It is a residue with a distinctive reddish color due to the presence of iron oxide of  $\text{Fe}_2\text{O}_3$ . Managing and finding environmentally sustainable solutions for the disposal of red mud is a significant challenge in the alumina refining industry [3][4][5]. It is generated in form of slurry and the dewatered form of red mud is known as bauxite residue [6]. On average, approximately 1.2 tons of bauxite residue is generated per ton of alumina produced. The annual generation of bauxite residue is above 150 million tons which was reported in the year of 2019 [7]. This generated bauxite residue quantity is influenced by various factors, including the processing parameters of the Bayer process and the origin of the bauxite ore. Globally, there is a stockpile of around 4.5 billion tons of bauxite residue [1]. Numerous utilization methods and strategies are under exploration to effectively manage and find potential applications for bauxite residue. These applications encompass the production of building materials, decorative tiles, and door filler materials. Additionally, bauxite residue is being investigated for its potential to extract valuable metal elements. Beyond industrial applications, it is being employed for environmental treatment and ecological restoration purposes. This includes its use in water purification, flue gas purification, soil improvement, bauxite residue reclamation, and

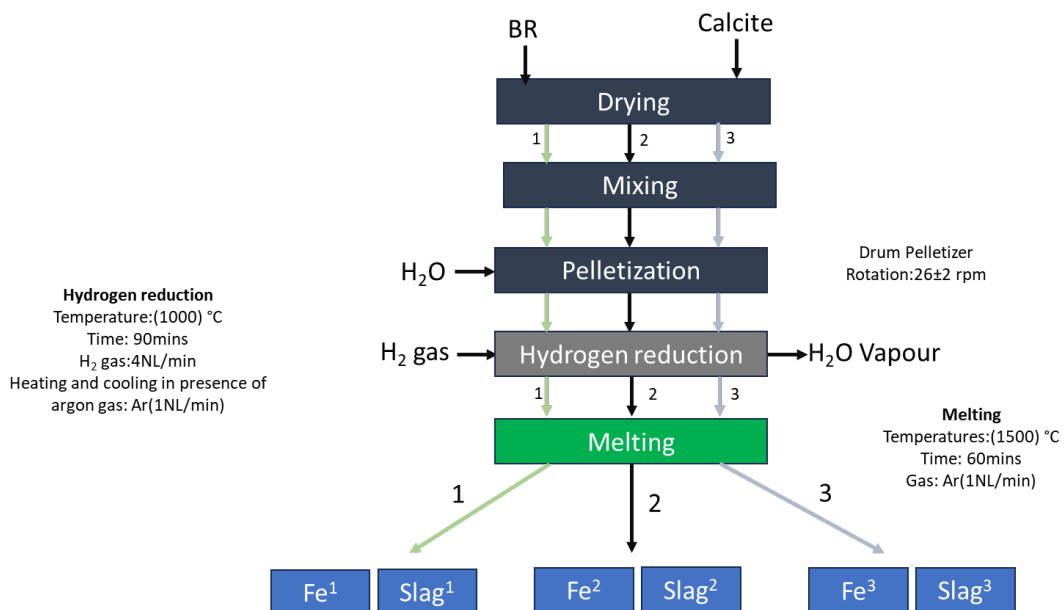
preparation for environmental restoration materials. The multifaceted potential of bauxite residue utilization highlights ongoing efforts to transform this byproduct into valuable resources across various domains [8]. Among these, all the utilization technology, various metal recovery from the bauxite residue will be the most economical. Many works are focusing on iron and alumina recovery from the bauxite residue through the carbothermic route [9][4].

In earlier studies, iron oxides were reduced to metallic iron utilizing carbon as a reductant. However, due to growing concerns about environmental greenhouse gas emissions, using carbon as a reductant has raised issues as it produces greenhouse gases during the reduction process. A more sustainable alternative to carbon is hydrogen, which serves as a reductant for iron oxide, leading to the production of water vapor as a byproduct, in contrast to the carbon monoxide (CO) and carbon dioxide (CO<sub>2</sub>) gases generated in carbothermic reduction.

The primary emphasis of this study lies in the examination of phase formation dynamics during the smelting process involving various bauxite residue calcite mixtures that have undergone hydrogen reduction. The investigation encompasses not only the separation of iron from the slag but also delves into the specific types of calcium aluminate phases (CaAl<sub>2</sub>O<sub>4</sub>, krotite) that manifest during the melting of the slag.

## 2. MATERIALS AND METHODS

The overall experimental processes of the research work have been presented in the Figure 1. Three different types of bauxite residue calcite pellets have been made and these are named as 1,2 and 3. The CaO:Al<sub>2</sub>O<sub>3</sub> (BR) mole ratio was varied 0.85, 1 and 1.15 to examine effect of CaO addition on the formation of calcium aluminate ,calcium silicate and calcium titanate phase during hydrogen reduction, and in the slag produced via a further smelting process.



1. Pellet composition(C<sub>0.85</sub>A)
2. Pellet composition(C<sub>1</sub>A)
3. Pellet composition(C<sub>1.15</sub>A)

Figure 1: Overall flow sheet of the experimental work.

### 2.1 Hydrogen reduction

Three distinct varieties of bauxite residue calcite were produced by employing a drum pelletizer, each characterized by different percentages of calcite. Following the pelletization process, these pellets underwent sintering at 1150 °C for 120 minutes to enhance their strength. The sintered pellets were subjected to hydrogen reduction in a TG (Thermogravimetric) furnace. The procedure involved

heating the sintered pellets in the presence of argon with a flow rate of 1 NI/min. Once the target temperature of 1000 °C was achieved, the gas flow was switched to hydrogen at a flow rate of 4 NI/min for 90 minutes. Upon completion of the reduction cycle, the reduced pellets were cooled to room temperature in an argon atmosphere. The heating, reduction, and cooling cycle was similar for all types of pellets. The XRD of the three different composition-reduced pellets are shown in Figure 2.

## 2.2 Smelting reduced pellets

Following the reduction process of various bauxite residue calcite pellets, smelting was conducted in a vertical tube furnace at 1500 °C for 60 minutes, maintaining an argon atmosphere. The primary objective of utilizing argon during the smelting process was to prevent the oxidation of metallic iron. The complete furnace description and working principle are described here [10]. An Alumina crucible was used to hold the samples.

## 2.3 Characterization

The phase analysis of slag was conducted through X-ray diffraction (XRD) using CuK $\alpha$  radiation (wavelength  $\lambda=1.54$  Å) on a Bruker AXS GmbH instrument in Karlsruhe, Germany. The diffractometer scanned within the 15° to 75° 2 $\theta$  range with a 0.03° step size. Qualitative phase analysis of the raw data employed DIFFRAC.EVA software with the PDF-4+ database (2014, ICDD, Philadelphia, Pennsylvania, USA). Standard samples for XRD were prepared by milling materials in a WC vibratory disk mill (RS 200, RETSCH GmbH, Haan, Germany) for 45 seconds at 800 revolutions per minute (rpm).

Quantitative analysis of phases, including krotite, gehlenite, and perovskite, utilized topas software based on the Rietveld method. To enhance quantitative analysis accuracy, specific parameters in the topas software, such as Zero error, LP(Lorentz–polarization) factor, sample displacement, and background, were adjusted. Microstructural analysis of the slags was conducted using a scanning electron microscope (SEM) (Zeiss Ultra FESEM) equipped with an XFlash® 4010 Detector from the Bruker Corporation for Energy-Dispersive X-Ray Spectroscopy (EDS). Energy dispersive spectroscopy (EDS) was employed to assess the elemental composition in various regions of the slags.

## 3. RESULTS AND DISCUSSION

### 3.1 Weight loss during hydrogen reduction

Figure 2 illustrates the weight loss over time for various compositions of bauxite residue calcite sintered pellets. It is evident from the figure that the weight loss is more pronounced for the C<sub>0.85</sub>A sintered pellets compared to the other two compositions. This higher weight loss can be attributed to the relatively higher fraction of iron oxide within the same mass of sintered pellets. On the other hand, the C<sub>1.15</sub>A pellets exhibit a higher initial rate of reduction, primarily due to their increased porosity. The elevated porosity of the C<sub>1.15</sub>A pellets stems from the higher percentage of CaCO<sub>3</sub> present, which undergoes decomposition during sintering, resulting in increased porosity. Theoretically, the weight loss should be greater for C<sub>1</sub>A pellets compared to C<sub>1.15</sub>A pellets. However,

the figure shows that the difference in weight loss between the two compositions is almost negligible.

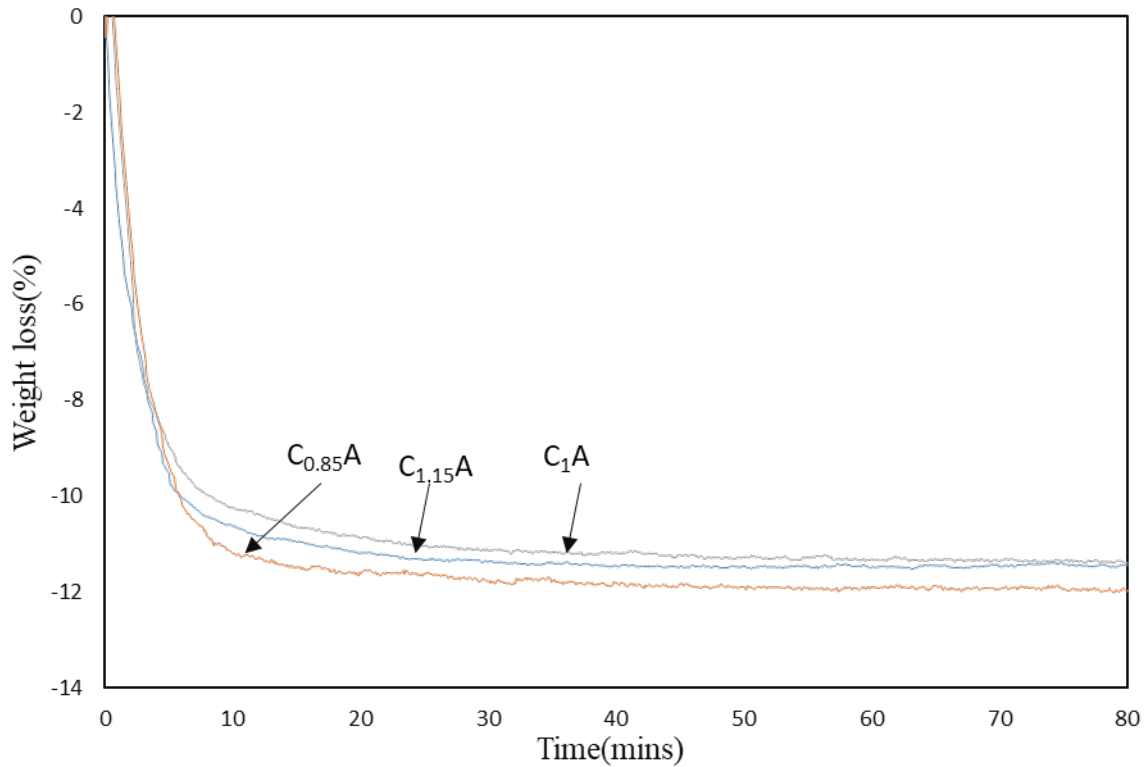


Figure 2: Weight loss vs Time for different composition bauxite residue calcite pellets (1000 °C, 4 NL/min H<sub>2</sub> flow rate)

### 3.2 Phase analysis of the reduced pellets and obtained slags

As depicted in Figure 3, the primary phases present in the reduced pellets include iron, mayenite, perovskite, larnite, gehlenite, and lime. These phases exhibit a consistent pattern across all the different compositions of bauxite residue-calcite reduced pellets, with variations in intensity observed among the different pellets.

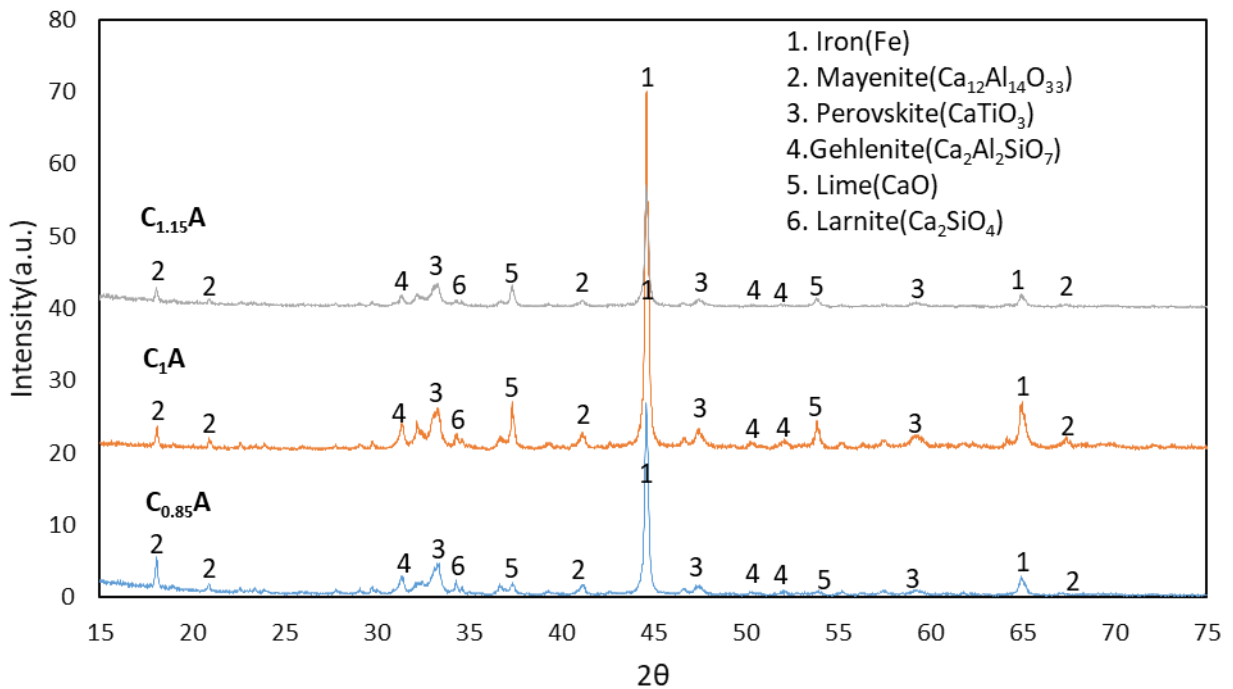


Figure 3: Phase analysis of different reduced pellets.

Figure 4 illustrates the phases formed in the slags obtained in the smelting of hydrogen-reduced bauxite residue-calcite pellets. Three primary phases, namely krotite ( $\text{CaAl}_2\text{O}_4$ ), gehlenite ( $\text{Ca}_2\text{Al}_2\text{SiO}_7$ ), and perovskite ( $\text{CaTiO}_3$ ), were identified in all smelted slag samples. Krotite emerged as the predominant phase in all the analyzed slag samples. From the quantitative XRD analysis, Krotite was high for the higher calcite-added pellets and lower for lower calcite pellets as shown in Table 1.

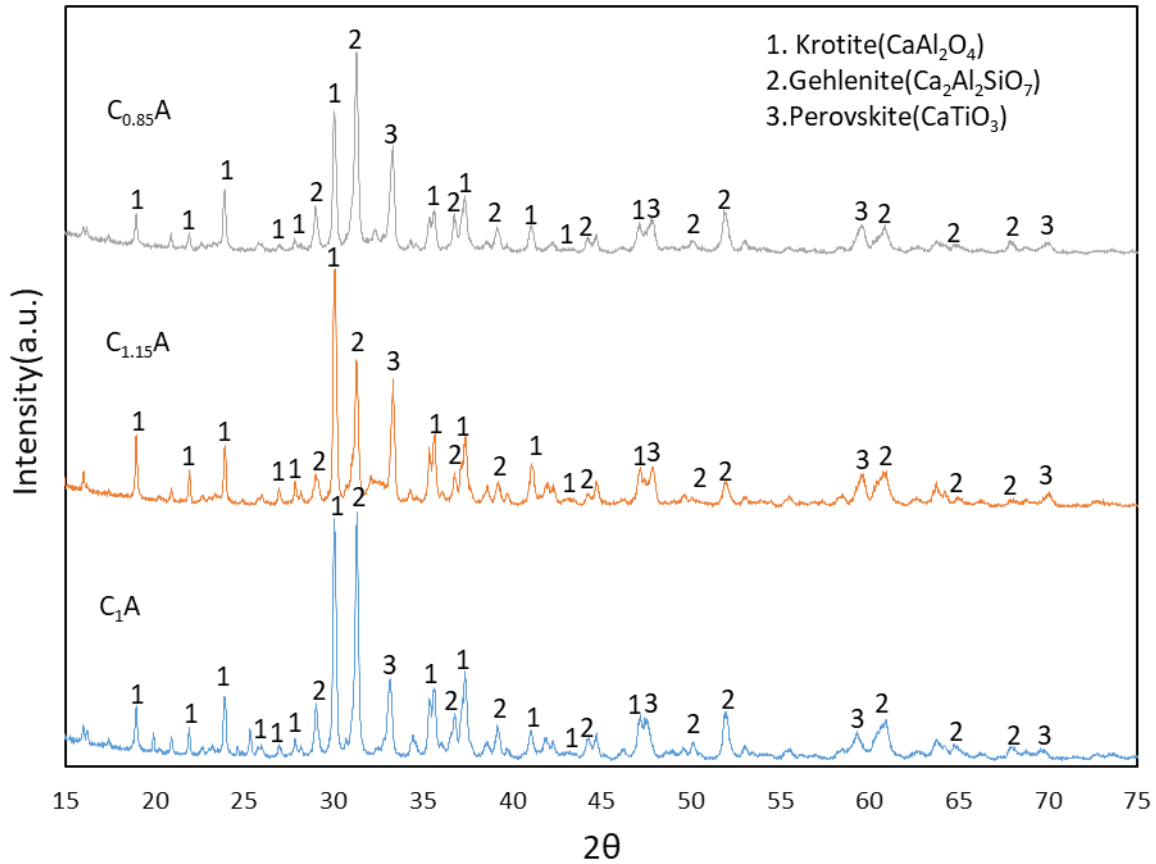


Figure 4: Phase analysis of different slags ( $C_1A$ ,  $C_{1.15}A$  and  $C_{0.85}A$ )

Table 1: Quantitative XRD analysis of the calcium aluminate phases in slags.

	$C_{0.85}A$	$C_1A$	$C_{1.15}A$
Gehlenite	17.94	15.41	8.38
Perovskite	10.53	9.89	5.67
Krotite	71.53	74.70	85.95

### 3.3 Microstructure

Figure 5 presents the elemental mapping of slag  $C_1A$ . As depicted in the figure, there is a significant overlap of calcium, aluminum, and oxygen in most areas, indicating the presence of krotite. This observation aligns with XRD data, where krotite constitutes a major fraction. In certain regions, the overlap of calcium, aluminum, silicon, and oxygen suggests the potential presence of the gehlenite phase. Additionally, the overlap of calcium, titanium, and oxygen is indicative of the perovskite phase. The presence of iron particles in the slag phase is notable, possibly resulting from incomplete iron separation due to the higher viscosity of the slag. The higher alumina fraction in the slag contributes to increased viscosity.

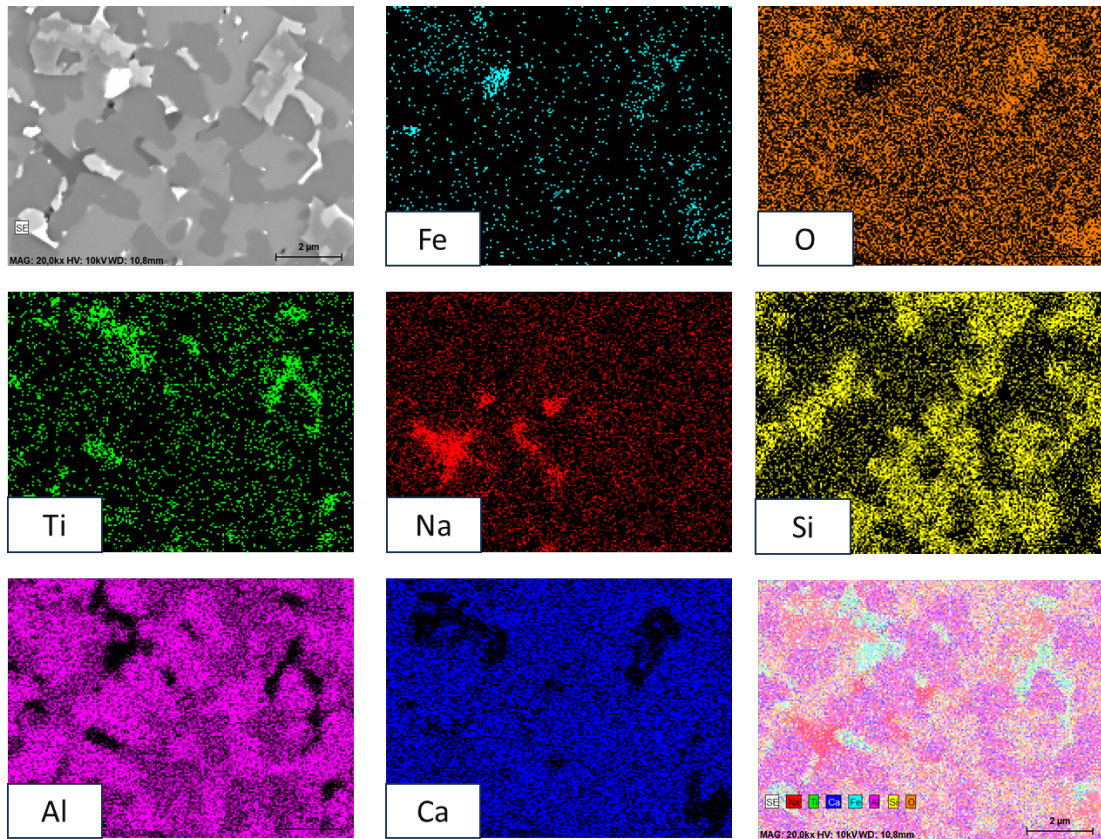


Figure 5: Elemental mapping of slag C<sub>1</sub>A.

Figure 6 displays the elemental analysis of the C<sub>1</sub>A slag and metals. On the left side of the figure, the bright areas represent pure iron. On the right side, three distinct phases are observed. The light grey phase consists predominantly of calcium, titanium, and oxygen, with a minor fraction of aluminum. This phase is likely the perovskite phase. The dark phase is composed of calcium, aluminum, and oxygen, with the addition of sodium, indicative of the krotite phase with some sodium present in the lattice. The light dark phase contains calcium, aluminum, oxygen, and silicon, representing the gehlenite phase.

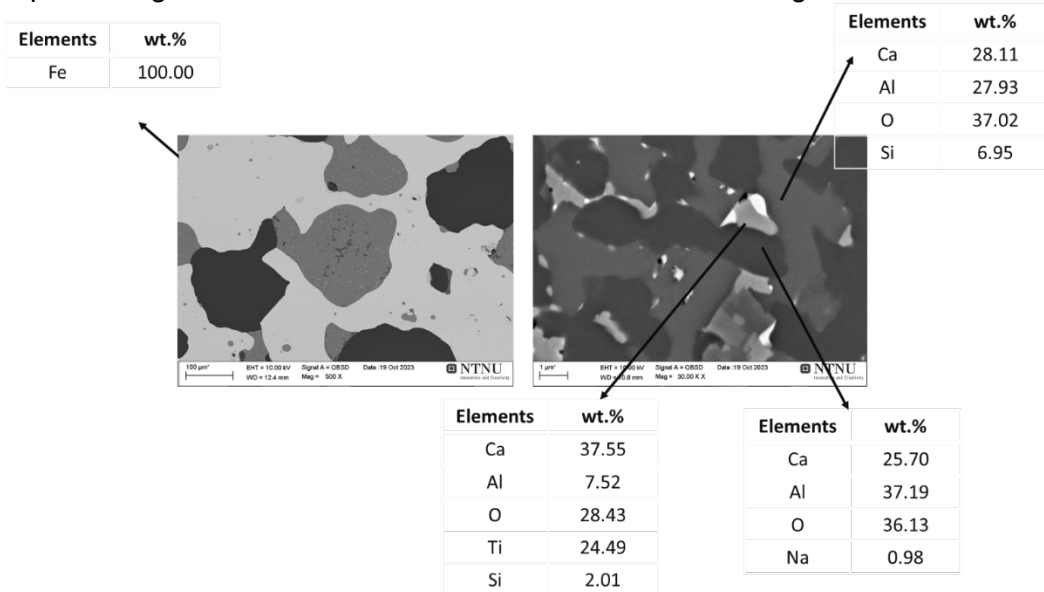


Figure 6: Elemental analysis of different phases of slag C<sub>1</sub>A.

The elemental mapping of  $C_{1.15}A$  and  $C_{0.85}A$  are similar (Figure 9 and Figure 7 respectively). However, it has difference in the amount of phases such as krotite, gehlenite, and perovskite, which is shown in the Table 1.

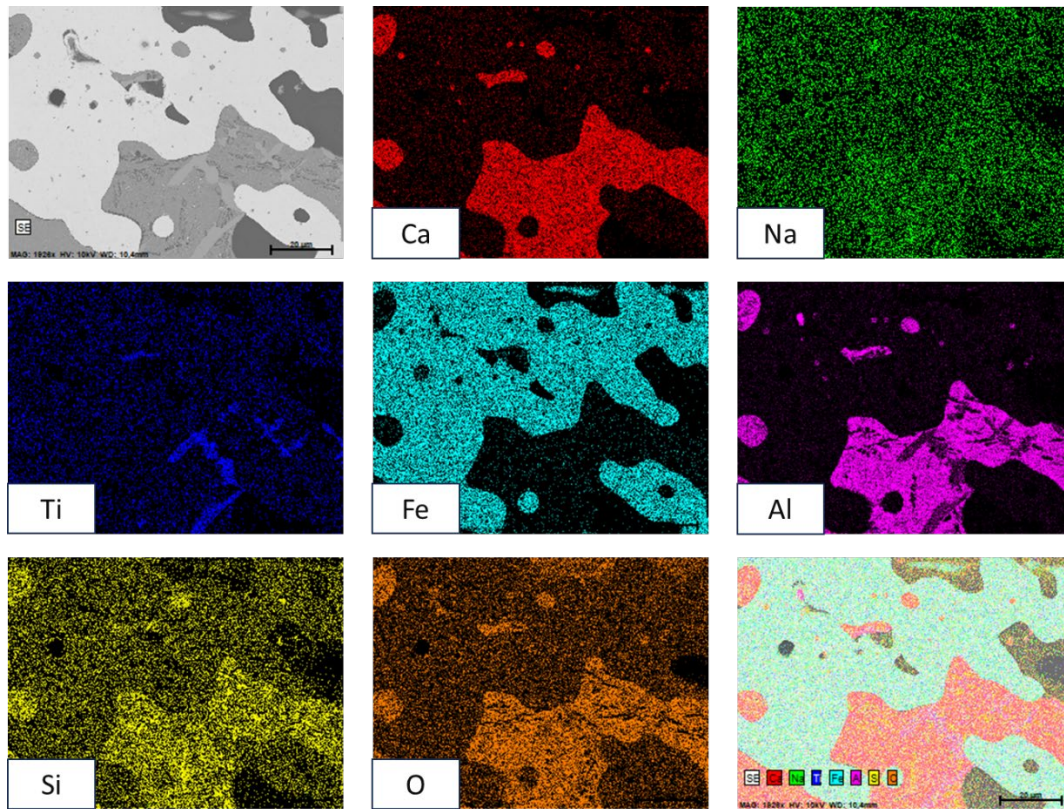


Figure 7: Elemental mapping of slag  $C_{0.85}A$ .

The elemental analysis of  $C_{0.85}A$  slag of different phases is shown in Figure 8. As shown in the figure white area are the metallic iron with little impurity of calcium, which is likely come from the surroundings signals as the elemental analysis area is smaller. Similar to the previous elemental analysis of  $C_1A$ , the light white area is the calcium titanate, and the dark area is the calcium aluminate. As shown in the right image of figure 8, the shrunk areas are the calcium silicate.

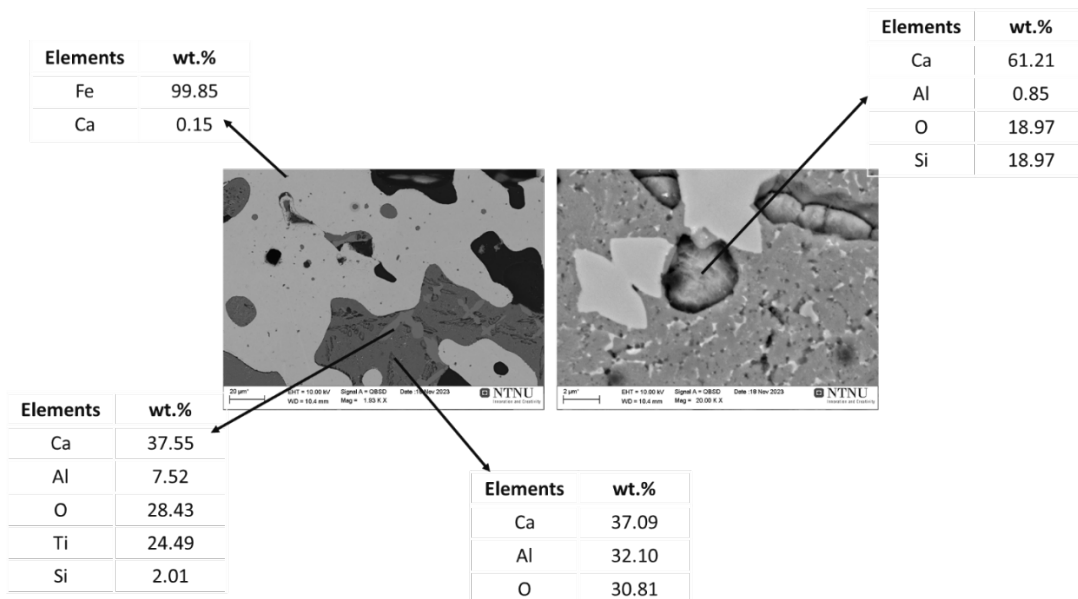


Figure 8: Elemental analysis of different phases of slag  $C_{0.85}A$ .

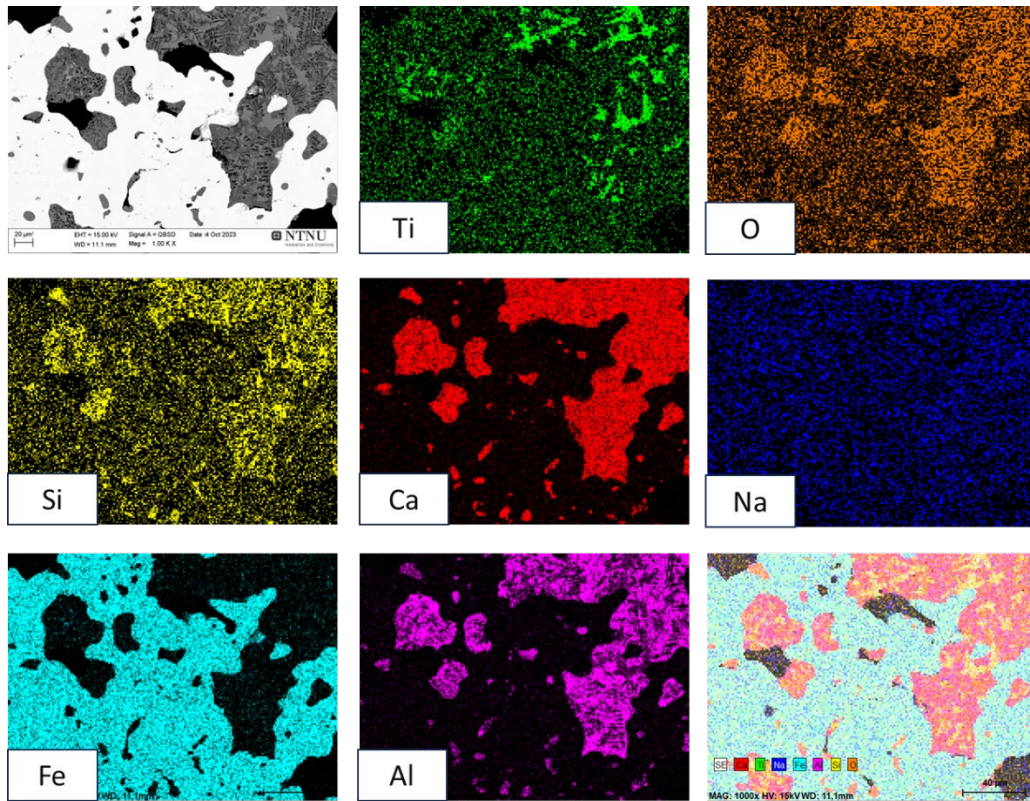


Figure 9: Elemental mapping of slag C<sub>1.15</sub>A.

Similar to Figure 8, the shrunk areas correspond to calcium silicate with a minor fraction of aluminum. The observed shrunk areas may be attributed to the higher volume shrinkage of calcium silicate compared to other phases, such as calcium aluminosilicate, calcium titanate, and calcium aluminat.

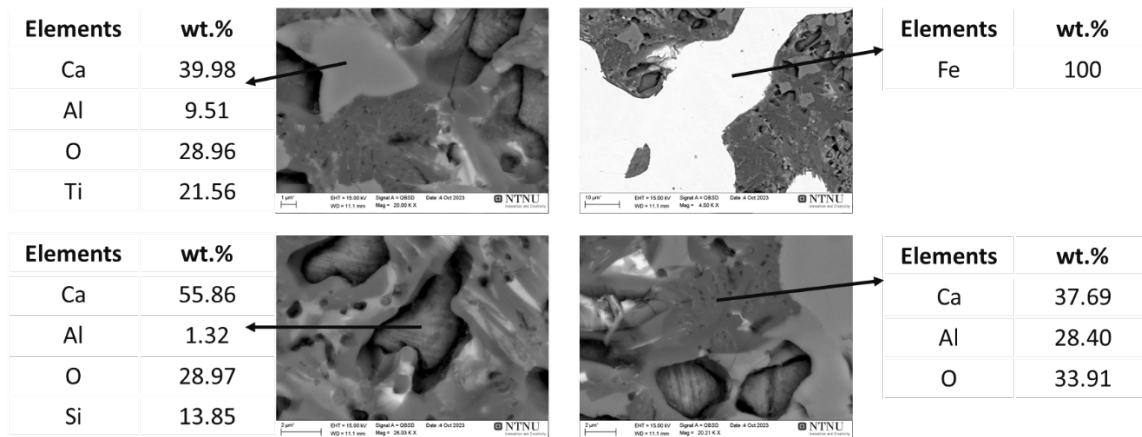


Figure 10: Elemental analysis of smelted slag of different phases C<sub>1.15</sub>A.

### 3.4 Phase formation

During the slags solidification after the smelting of the reduced pellets of different bauxite residue-calcite pellets, three major phases formed in the slag are krotite, perovskite, and gehlenite. The phases formed are as follows:



Thermodynamic calculations of slag phases were performed using Factsage 8.1 with the FT oxide database. The calculation considered four major oxides from actual measurements in experimental work, namely CaO, Al<sub>2</sub>O<sub>3</sub>, SiO<sub>2</sub>, and TiO<sub>2</sub>. Notably, sodium oxide (Na<sub>2</sub>O) was excluded from these

calculations due to observed sodium losses during hydrogen reduction [11]. The thermodynamic calculations were conducted at a temperature of 1500 °C and a pressure of 1 atm, mirroring the experimental conditions.

The Scheil-Gulliver cooling model was selected for thermodynamic calculations, chosen for its faster cooling rate. Figure 11 illustrates that the major phases identified in the calculation include  $\text{CaAl}_2\text{O}_4$ ,  $\text{Ca}_3\text{Al}_2\text{O}_6$ ,  $\text{Ca}_2\text{SiO}_4$ , and  $\text{Ca}_3\text{Ti}_2\text{O}_7$ . However, in the experimental analysis, the calcium aluminate phase was observed in krotite form, calcium aluminosilicate manifested in gehlenite, and calcium titanate appeared in perovskite form. The observed variation in phases between experimental and thermodynamic calculations may be attributed to the faster cooling rate of the slag and the interactions between high-temperature slag with the crucible.

Gehlenite phase was not found in the thermodynamics calculation may be due to the dissociation of gehlenite to calcium silicate and alumina. The reaction equation is as follows:

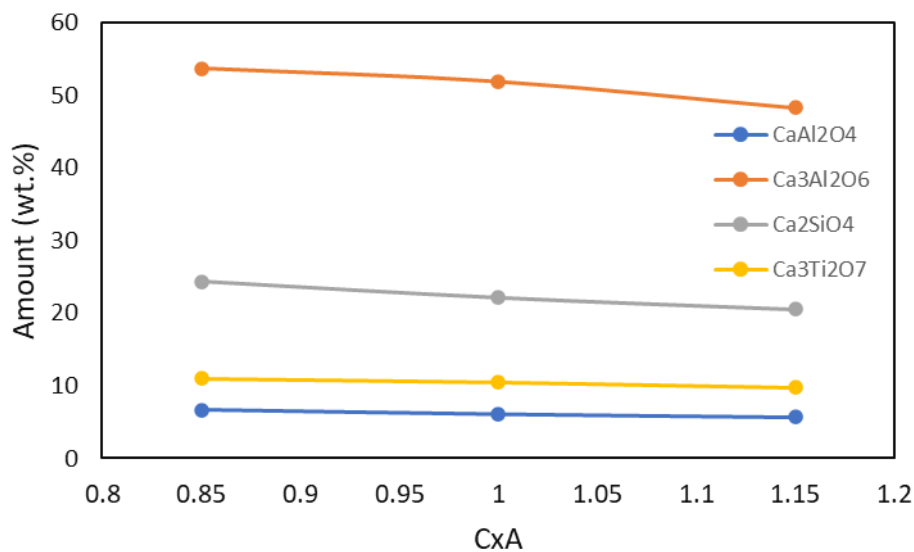


Figure 11: Phase fraction of different phases calculated by using FactSage 8.1.

## 4.0 CONCLUSION

The following conclusions from the hydrogen reduction and smelting of different mixtures of bauxite residue and calcite:

1. Metallic iron and mayenite dominate as the major phases in the reduced pellets. The phases formed in the reduced pellets from different bauxite residue calcite compositions exhibit similarities with variations in phase fraction.
2. Following the smelting of distinct reduced pellets, the primary phases observed in the resulting slag include krotite, gehlenite, and perovskite.
3. The leachable calcium aluminate phase, identified as krotite, is present in higher quantities in the pellets with higher calcite content, as revealed by quantitative phase analysis of the slag.
4. Thermodynamic calculations indicate that the major phases anticipated in the slag are  $\text{CaAl}_2\text{O}_4$ ,  $\text{Ca}_3\text{Al}_2\text{O}_6$ ,  $\text{Ca}_2\text{SiO}_4$ , and  $\text{Ca}_3\text{Ti}_2\text{O}_7$ . Discrepancies between experimental and thermodynamic results may be attributed to the faster cooling rate and interactions during the melting process, including those with the alumina crucible, which could introduce variations in the outcomes.
5. The iron purity achieved during the smelting of the reduced pellets exceeds 99.0 wt.%.

## ACKNOWLEDGEMENTS

This study was performed and financially supported by The European Union's Horizon 2020 research and innovation program under grant number of 958307 (HARARE project).

## REFERENCES

- [1] M. K. Kar, M. A. R. Önal, and C. R. Borra, "Alumina recovery from bauxite residue: A concise review," *Resour. Conserv. Recycl.*, vol. 198, p. 107158, 2023.
- [2] M. K. Kar, A. Hassanzadeh, C. van der Eijk, P. B. Kowalczuk, K. Aasly, and J. Safarian, "Properties of self-hardened CaO-added bauxite residue pellets, and their behavior in hydrogen reduction followed by leaching and magnetic separation for iron and alumina recovery," *Int. J. Hydrogen Energy*, 2023.
- [3] K. Evans, E. Nordheim, and K. Tsesmelis, "Bauxite residue management," *Light Met.* 2012, pp. 63–66, 2016.
- [4] A. Lazou, C. Van der Eijk, E. Balomenos, L. Kolbeinsen, and J. Safarian, "High temperature smelting reduction of bauxite residue and a CaCO<sub>3</sub>-rich bauxite for aluminat slag production and pig iron recovery," in *Proceedings of the 3rd International Bauxite Residue Valorisation and Best Practices Conference, Virtual*, 2020, pp. 77–83.
- [5] C. Cardenia, E. Balomenos, and D. Panias, "Iron recovery from bauxite residue through reductive roasting and wet magnetic separation," *J. Sustain. Metall.*, vol. 5, no. 1, pp. 9–19, 2019.
- [6] M. K. Kar and J. Safarian, "Characteristics of Bauxite Residue–Limestone Pellets as Feedstock for Fe and Al<sub>2</sub>O<sub>3</sub> Recovery," *Processes*, vol. 11, no. 1, p. 137, 2023.
- [7] M. Archambo and S. K. Kawatra, "Red mud: Fundamentals and new avenues for utilization," *Miner. Process. Extr. Metall. Rev.*, pp. 1–24, 2020.
- [8] X. Chao, T. Zhang, G. Lv, Y. Chen, X. Li, and X. Yang, "Comprehensive application technology of bauxite residue treatment in the ecological environment: a review," *Bull. Environ. Contam. Toxicol.*, pp. 1–6, 2022.
- [9] K. E. Ekstrøm, A. V. Bugten, C. van Der Eijk, A. Lazou, E. Balomenos, and G. Tranell, "Recovery of iron and aluminum from bauxite residue by Carbothermic reduction and slag leaching," *J. Sustain. Metall.*, vol. 7, no. 3, pp. 1314–1326, 2021.
- [10] A. Rasouli, K. E. Herstad, J. Safarian, and G. Tranell, "Magnesiothermic Reduction of Natural Quartz," *Metall. Mater. Trans. B*, vol. 53, no. 4, pp. 2132–2142, 2022.
- [11] M. K. Kar, C. van der Eijk, and J. Safarian, "Kinetics Study on the Hydrogen Reduction of Bauxite Residue-Calcite Sintered Pellets at Elevated Temperature," *Metals (Basel)*, vol. 13, no. 4, p. 644, 2023.